

Contents lists available at ScienceDirect

Polymer

journal homepage: http://www.elsevier.com/locate/polymer





Influence of counteranion and humidity on the thermal, mechanical and conductive properties of covalently crosslinked ionenes

Nicholas C. Bontrager, Samantha Radomski, Samantha P. Daymon, R. Daniel Johnson, Kevin M. Miller *

1201 Jesse D. Jones Hall, Department of Chemistry, Murray State University, Murray, KY, 42071, USA

ARTICLE INFO

Keywords: Ionene Crosslinked network Ionic conductivity

ABSTRACT

Thiol-ene photopolymerization was used to generate a series of covalently crosslinked, imidazolium-containing ionene networks. A variety of counteranions were chosen so as to investigate the influence of size and basicity on the thermal, mechanical and conductive properties of the resulting networks. Anhydrous conductivities at $20\,^{\circ}$ C were found to be on the order of 10^{-6} to 10^{-10} S/cm and correlated to some degree with T_g ; however, T_g -normalization of the curves indicated that this relationship between polymer structure and conductivity was more complex. VFT fitting, along with free ion concentration and ion mobility data, were investigated in order to provide additional insight. Also of interest in this study was the influence of humidity on ionic conductivity. Hydrophilic networks with anions such as [Cl], [NO₃] or [OMs] were found to exhibit 3- to 5-orders of magnitude enhancement in ionic conductivity (up to 10^{-3} S/cm) when the relative humidity was increased to 70% while the more hydrophobic networks ([PF₆] and [NTf₂]) were not influenced. Further experimentation (water uptake, DSC) indicated that the observed enhancements in conductivity were likely due to a combination of plasticization and water-assisted ion transport.

1. Introduction

Poly(ionic liquid)s (PILs) are a sub-class of ion-conducting polymers wherein a pendant ionic liquid (IL) or ionic group is in the repeating unit [1–3]. Ionenes represent another class of ionic polymers where the ionic liquid or ionic group is located directly in the backbone of the repeating unit [4,5]. Both PILs and ionenes attempt to combine the best properties of both ILs (excellent thermal and conductive properties) and the macromolecular architecture (mechanical stability) in which the IL monomer is incorporated. The synthetic versatility of available IL monomers in recent years has led to an exponential growth in new polymer architectures and thus prospective applications have likewise expanded. Examples of such applications include alkaline and ion exchange membranes (AEMs/IEMs) [6-13], gas separation membranes [14-19], and solid electrolytes [20-22]. One underlying theme throughout these studies is that new polymer designs must continue to be explored in order to meet the demand for materials with higher ionic conductivities and improved thermal, chemical and mechanical

Since one of the ions (typically the cation) is covalently bound into

the repeating unit, PILs and ionenes act as single ion transporters. Ionic conductivity is influenced by a number of factors, including the concentration and mobility of the ion, polymer morphology and polymer chain relaxation (often reflected in the glass transition temperature (T_g)). As a result, a number of unique challenges to the design of improved ionic polymer structures exist. It is generally accepted that the use of larger, non-coordinating counterions improve segmental dynamics (reflected by a reduction in T_g), increasing anhydrous conductivity [22,23]. On the other hand, some end-use applications which require an aqueous medium, such as AEMs and proton exchange membranes (PEMs), actually prefer ions that result in more hydrophilic networks. In an aqueous environment, the interplay between absorbed water, polymer structure and ion transport is complex [24], and hydrophilic polymers which contain anions such as halides, hydroxide, alkoxides, and other inorganic anions are advantageous in that they often result in ion-containing polymers that exhibit increased water permeability and absorptivity. However, several of these hydrated systems suffer from a lack of mechanical stability. Still, under hydrated conditions, more hydrophilic polymers often exhibit ionic conductivities several orders of magnitude higher than under anhydrous conditions.

E-mail address: kmiller38@murraystate.edu (K.M. Miller).

^{*} Corresponding author.

For example, Elabd et al. demonstrated a 3-4 orders of magnitude increase in bromide conductivity when increasing the relative humidity from 25 to 90% in a series of PIL block copolymers where one of the blocks contained an imidazolium moiety in the repeating unit [12,25]. Such an effect was attributed to a NafionTM-like, water-assisted ion transport mechanism, meaning that transport in these systems is less dependent upon polymer chain dynamics versus anhydrous conditions [25,26]. Ion-rich microdomains were found to form within the block copolymer morphology at intermediary humidity (as deduced from x-ray scatting experiments), increasing ion transport through the creation of ion channels. Madsen et al. recently applied NMR diffusometry as a method to further decipher water transport, utilizing as examples ammonium hydroxide and bromide PILs as well as anionic sulfonated poly(ether sulfone)s [27]. As these polymers absorbed water, local, nanometer scale cavities became increasingly interconnected (reduced tortuosity), leading to improved ion transport and higher conductivity. However, the authors noted that, on the micrometer (bulk) scale, ion transport could be hindered by the clustering of hetereogenous "dead-end" pathways.

From a synthetic perspective, the majority of imidazoliumcontaining PILs have been prepared through the polymerization of vinyl-, (meth)acrylic- or styrenyl-substituted IL monomers. Step-growth strategies used to generate ionenes are less common, although several examples have utilized S_N2, polyurethane or polyesterification chemisty [28–31]. In all of these cases, conductivities of up to 10^{-5} S/cm at 25 °C were observed, despite the imidazolium group being anchored directly into the polymer backbone. Furthermore, Segalman et al. observed that a imidazolium-containing, step-growth ionene ("backbone" PIL) exhibited significantly higher ionic conductivity (4-orders of magnitude) over a similar "pendant" PIL [32]. This study demonstrated that thoughtful synthesis of ionene architecture could create a more continuous ionic matrix (termed "percolated aggregates"), leading to improved ion transport and conductivity, a concept which has been supported by theoretical simulations [33-35]. However, it should be pointed out that the role and extent of ion aggregation in ionic polymers, regardless of their structure, is still not well understood.

Covalently crosslinked networks provide another synthetic approach towards producing ionic polymers with percolated aggregates and potentially improved ionic conductivity. Although creating a network could be a deterrent for improved ionic conductivity as the single ion conductors could face a difficult pathway of hopping from one binding site to another, strategic placement of said ions and their covalently bound counterions could create the aforementioned percolated domains. Evans et al. recently correlated ion aggregation and conductivity of ammonium-containing, linear and covalently crosslinked network ionenes bearing bis(trifluoromethylsulfonyl)imide) [NTf2] counteranions [36]. The network bearing a longer undecyl (C11) linker was found to exhibit the highest T_g -independent conductivity and the strongest ion aggregation, supported by WAXS data. The authors hypothesized that this network exhibited an enhanced conductivity due to a higher degree of percolated aggregate domains.

We have also investigated ionene networks, although primarily as a way to improve the mechanical stability of ionic polymers. Basecatalyzed Michael addition polymerization was first utilized to couple imidazolium or triazolium-containing acetoatetate monomers with difunctional acrylates. Many of these systems exhibited better than expected ionic conductivites (up to 10^{-5} at 30 °C/30% RH) [37,38]. Thiol-ene photochemistry has more recently been utilized, leading to a much more versatile group of networks with controllable crosslink density [39,40]. These studies indicated that, even with high degrees of crosslink density and excellent mechanical stability, ionic conductivities were found to be very reasonable (10^{-5} - 10^{-7} S/cm at 30 °C, 30% RH). In the present work, we turn our attention to the influence of counteranion on the thermal, mechanical and conductive properties of imidazolium-containing, ionene networks, prepared using thiol-ene photochemistry. All networks reported here were prepared keeping a

stoichiometric ratio of thiol and ene functional groups so as to achieve a high degree of crosslink density and mechanical stability. Counteranions studied encompassed a rather wide scope in terms of size and network hydrophilicity ([Cl], [NO₃], [OMs], [OTf], [ClO₄], [PF₆] and [NTf₂]) as one of our additional goals was to study the effect of relative humidity on ionic conduction. Anhydrous conductivity of the networks was found to correlate inversely with the T_g of the networks with rubbery plateau moduli (E') values of 5.7–7.5 MPa. Hydrophilic networks which contained anions such as [Cl], [NO₃] or [OMs] were observed to have 3- to 5-orders of magnitude enhancements in ionic conductivity when the relative humidity was increased from 0 to 70% while hydrophobic anions such as [PF₆] and [NTf₂] exhibited no observable change.

2. Experimental section

General. All chemicals were purchased from Sigma-Aldrich or Acros Organics and were used as received without further purification. Pentaerythritol tetrakis(3-mercaptopropionate) (PTMP, > 95%) was placed in a high vacuum oven (50 °C, < 0.01 mm Hg) for 48 h prior to use. An ELGA Purelab® Ultra filtration device produced ultrapure water having a resistivity of 18 M Ω -cm. The syntheses of sodium imidazole [41] and 6-iodohex-1-ene [42] have been previously reported.

Synthesis of 1-(hex-5-enyl)imidazole 1. To a single-necked, 250-mL round bottomed flask was suspended sodium imidazole [41] (4.00 g, 44.4 mmol) in anhydrous THF (100 mL). To this magnetically stirred mixture was added 6-iodohex-1-ene [42] (10.26 g, 48.9 mmol). The resulting mixture was warmed to reflux and stirred for 24 h. The reaction was then cooled to room temperature, filtered, and the solvent removed under reduced pressure to afford a yellow residue which was subsequently taken up into chloroform (100 mL) and washed with DI water (50 mL). The organic phase was separated, washed with additional DI water and brine (50 mL each), dried over a mixture of Na₂SO₄/MgSO₄, filtered, and the solvent removed under reduced pressure to afford a crude yellow oil. Purification by column chromatography on silica gel with a gradient elution of 10-50% acetone in hexanes provided 4.69 g (71%) of a light yellow oil. ¹H NMR (400 MHz, CDCl₃): δ 7.38 (s, 1H), 6.97 (s, 1H), 6.82 (s, 1H), 5.67 (m, 2H), 4.85-4.94 (m, 4H), 3.85 (t, 4H, J = 7.3 Hz), 1.98 (m, 4H), 1.70 (m, 4H), 1.31 (m, 4H). 13 C NMR (100 MHz, CDCl $_3$): δ 137.6, 136.8, 129.2, 118.6, 115.0, 46.7, 32.9, 30.2, 25.5. Anal. Calcd. for $C_9H_{14}N_2$: C 71.96, H 9.39, N 18.65. Found: C 71.82, H 9.33, N 18.78.

Synthesis of 1,3-bishexenylimidazolium chloride 2a. To a 50-mL round bottomed flask equipped with a magnetic stir bar was charged 1-(hex-5-enyl)imidazole 1 (4.25 g, 28.3 mmol) and 6-chlorohex-1-ene (3.36 g, 28.3 mmol). The mixture was warmed to 60 °C and stirred for 5 days. The reaction was cooled to room temperature, then washed with diethyl ether (3 \times 25 mL) and dried under high vacuum, affording a viscous, light brown oil (6.70 g, 88%). $^{1}{\rm H}$ NMR (400 MHz, DMSO- $d_{\rm 6}$): δ 9.35 (s, 1H), 7.83 (s, 2H), 5.77 (m, 2H), 4.96–5.05 (m, 4H), 4.18 (t, 4H, J=7.1 Hz), 2.04 (m, 4H), 1.78 (m, 4H), 1.30 (m, 4H). $^{13}{\rm C}$ NMR (100 MHz, DMSO- $d_{\rm 6}$): δ 138.1, 136.1, 122.5, 115.2, 48.6, 32.4, 28.8, 24.7. Anal. Calcd. for C15H25ClN2: C 67.02, H 9.37, N 10.42. Found: C 66.81, H 9.44, N 10.62.

Synthesis of 1,3-bishexenylimidazolium ILs 2b-e from metathesis with silver salts ([NO₃], [OMs], [OTf] and [PF₆]). Generally, in a 100-mL round bottomed flask equipped with a magnetic stir bar was dissolved 1,3-bishexenylimidazolium chloride 2a (2.00 g, 7.44 mmol) in DI water (20 mL) A solution of the desired silver salt (7.59 mmol) in DI water (10 mL) was then added and the resulting mixture was stirred in the dark overnight. Dichloromethane (20 mL) was then added and stirring continued for 1 h. The entire mixture was then filtered through Celite, followed by isolation of the organic phase. The solvent was removed under reduced pressure to afford a series of light yellow oils.

1,3-Bishexenylimidazolium nitrate 2a. (1.95 g, 89%). 1 H NMR (400 MHz, DMSO- 4 G): δ 9.25 (s, 1H), 8.12 (s, 2H), 5.77 (m, 2H), 4.94–5.04 (m, 4H), 4.18 (t, 4H, J = 7.3 Hz), 2.03 (m, 4H), 1.79 (m, 4H), 1.31 (m,

4H). ^{13}C NMR (100 MHz, DMSO- d_6): δ 138.1, 136.0, 122.5, 115.2, 48.7, 32.4, 28.8, 24.7. Anal. Calcd. for $C_{15}H_{25}N_3O_3$: C 60.99, H 8.53, N 14.23. Found: C 61.14, H 8.59, N 13.95.

1,3-Bishexenylimidazolium mesylate 2c. (2.23 g, 91%). 1 H NMR (400 MHz, DMSO-d₆): δ 9.28 (s, 1H), 7.82 (s, 2H), 5.77 (m, 2H), 4.95–5.05 (m, 4H), 4.19 (t, 4H, J=7.3 Hz), 2.31 (s, 3H), 2.04 (m, 4H), 1.80 (m, 4H), 1.31 (m, 4H). 13 C NMR (100 MHz, DMSO-d₆): δ 138.7, 136.7, 123.1, 115.8, 49.3, 40.4, 33.0, 29.4, 25.3. Anal. Calcd. for C₁₆H₂₈N₂O₃S: C 58.50, H 8.59, N 8.53, S 9.76. Found: C 58.64, H 8.62, N 8.62, S 9.88.

1,3-Bishexenylimidazolium triflate 2d. (2.65 g, 93%). 1 H NMR (400 MHz, DMSO- 4 G): δ 9.19 (s, 1H), 7.80 (s, 2H), 5.77 (m, 2H), 4.93–5.04 (m, 4H), 4.17 (t, 4H, 2 J = 7.1 Hz), 2.04 (m, 4H), 1.80 (m, 4H), 1.31 (m, 4H). 13 C NMR (100 MHz, DMSO- 4 G): δ 138.1, 135.9, 122.5, 120.6 (q, 2 J = 322 Hz, -CF₃), 115.2, 48.7, 32.4, 28.8, 24.7. Anal. Calcd. for C₁₆H₂₅F₃N₂O₃S: C 50.25, H 6.59, N 7.32, S 8.38. Found: C 50.33, H 6.54, N 7.40, S 8.32.

1,3-Bishexenylimidazolium hexafluorophosphate 2e. (2.02 g, 96%). 1 H NMR (400 MHz, DMSO- d_{6}): δ 9.18 (s, 1H), 7.79 (s, 2H), 5.78 (m, 2H), 4.94–5.05 (m, 4H), 4.17 (t, 4H, J=7.1 Hz), 2.04 (m, 4H), 1.80 (m, 4H), 1.31 (m, 4H). 13 C NMR (100 MHz, DMSO- d_{6}): δ 138.1, 135.9, 122.5, 115.2, 48.7, 32.4, 28.8, 24.7. Anal. Calcd. for $C_{15}H_{25}F_{6}N_{2}P$: C 47.62, H 6.66, N 7.40. Found: C 47.79, H 6.57, N 7.37.

2.1. Synthesis of 1,3-bishexenylimidazolium perchlorate 2e

Following a procedure by Welton et al. [43], sodium perchlorate (1.00 g, 8.20 mmol) was added to a solution of 1,3-bishexenylimidazolium chloride 2a (2.00 g, 7.45 mmol) in dichloromethane (25 mL) and the resulting mixture was magnetically stirred for 24 h. The mixture was filtered and the organic filtrate was washed multiple times with DI water (3 \times 20 mL) until the organic solution resulted in no precipitate formation as the result of concentrated silver nitrate solution addition. The solvent was then removed under reduced pressure to afford the desired perchlorate 2e as a light yellow oil (2.29 g, 92%). $^1\mathrm{H}$ NMR (400 MHz, DMSO-d₆): δ 9.18 (s, 1H), 7.80 (s, 2H), 5.77 (m, 2H), 4.94–5.04 (m, 4H), 4.17 (t, 4H, J=7.1 Hz), 2.04 (m, 4H), 1.79 (m, 4H), 1.31 (m, 4H). $^{13}\mathrm{C}$ NMR (100 MHz, DMSO-d₆): δ 138.1, 136.0, 122.5, 115.2, 48.7, 32.4, 28.8, 24.7. Anal. Calcd. for $C_{15}\mathrm{H}_{25}\mathrm{ClN}_2\mathrm{O}_4$: C 54.13, H 7.57, N 8.42. Found: C 54.13, H 7.33, N 8.45.

Synthesis of 1,3-bishexenylimidazolium bis(trifluoromethylsulfonyl) imide 2f. To a 100-mL round-bottomed flask was dissolved 1,3-bishexenylimidazolium chloride 2a (2.00 g, 7.44 mmol) in DI water (20 mL). A solution of lithium bis(trifluoromethylsulfonyl)imide (2.17 g, 7.59 mmol) in DI water (10 mL) was then added and the resulting mixture was stirred overnight. The mixture was poured onto chloroform (30 mL) and the organic phase was isolated and washed with DI water (3 \times 25 mL), followed by removal of the solvent under reduced pressure. The reaction yielded 2f as a light yellow oil (3.64 g, 95%). $^1\mathrm{H}$ NMR (400 MHz, DMSO-d₆): δ 9.19 (s, 1H), 7.79 (s, 2H), 5.77 (m, 2H), 4.96–5.05 (m, 4H), 4.17 (t, 4H, J=7.3 Hz), 2.04 (m, 4H), 1.80 (m, 4H), 1.32 (m, 4H). $^{13}\mathrm{C}$ NMR (100 MHz, DMSO-d₆): δ 138.0, 136.0, 122.5, 119.4 (q, J=319 Hz, $-\mathrm{CF}_3$), 48.7, 32.4, 28.8, 24.7. Anal. Calcd. for $\mathrm{C}_{17}\mathrm{H}_{25}\mathrm{F}_6\mathrm{N}_3\mathrm{O}_4\mathrm{S}_2$: C 39.76, H 4.91, N 8.18, S 12.49. Found: C 39.89, H 4.87, N 8.37, S 12.71.

Monomer Characterization. ^1H and ^{13}C NMR spectra were obtained on a JEOL-ECS 400 MHz spectrometer and reported chemical shift values were referenced to residual solvent signals (CDCl₃: ^1H , 7.26 ppm; ^{13}C , 77.16 ppm; DMSO- ^4G : ^1H , 2.50 ppm; ^{13}C , 39.52 ppm). Relevant NMR spectra are included in the Supporting Information. Elemental analyses were completed on a PerkinElmer 2400 CHNS/O Series II Elemental Analyzer. Residual chloride [Cl] concentrations in ILs 2b-g were determined by ion chromatography (ICS-1100, Dionex) as follows: an eluent concentration of 4.5 mM $^2\text{CO}_3^2$ Mm ^2M HCO $_3^2$ with a flow rate of 1.2 mL/min and a suppressor current of 31 mA. Chromatographic calibration was accomplished via the preparation and analysis of aqueous standards prepared by serial dilution of a 1000 ppm

[Cl] stock solution (from sodium chloride, Aldrich, > 99.9%). Each IL (10–15 mg) was dissolved in 1 mL of acetonitrile and injected. The amount of residual chloride in ionic ILs 2b-g was determined to be less than 0.01% w/w.

Photopolymerization Procedure. Covalently crosslinked ionene networks were prepared following a previously published procedure from our laboratory [39]. The thiol:ene functional group ratio was stoichiometric for all of the photopolymerizations. In the dark, 1 wt % of the photoinitiator diphenyl(2,4,6-trimethylbenzoyl)phosphine oxide (TPO, 9.6 mg) was dissolved, with light heating, in PTMP (1.0 mmol). The appropriate 1,3-bishexenylimidazolium IL monomer (2.0 mmol) was then added and the resulting mixture was shaken using a vortex mixer until a clear solution was obtained. The monomer solution was dispensed by syringe between two Rain-X® treated glass slides, separated by a 0.5 mm PTFE spacer, held together by binder clips, followed by exposure to a broadband UV lamp (UVP Blak-Ray $^{\rm TM}$ B-100AP High-Intensity UV Lamp) for 5 min on each side. The resulting polymer films were stored in a vacuum oven (60 °C, < 0.1 mm Hg) for a minimum of 24 h prior to analysis.

Polymer Characterization. A PerkinElmer Spectrum Two™ FT-IR in transmission mode was utilized to record infrared spectra. The PerkinElmer Spectrum 10TM software was used to follow the desired peaks at 1 cm⁻¹ resolution using 32 scans. Multiple FTIR spectra were taken for each thiol-ene network specimen before and after UV curing and thiol (2570 cm⁻¹) and double bond (1630 cm⁻¹) conversions were determined following a literature reported method [44]. Error in measurements was determined to be less than \pm 2%. Gel fraction experiments were accomplished in triplicate on each PIL network using Soxhlet extraction in THF (24 h reflux) and calculations (gel fraction, % swelling) were completed according to a previously published method [45]. A TA Instruments Q200 differential scanning calorimeter (DSC) was used to determine the glass transition temperature (T_g) from the inflection point for each network from the second heating event at a heating rate of 2 °C/min on 4–8 mg samples (error of ± 2.0 °C from duplicate runs). Thermal stability ($T_{d5\%}$) studies were completed in duplicate on each polymer sample using a TA Instruments Q500 thermogravimetric analyzer (TGA) at a heating rate of 10 °C/min under a constant dry nitrogen flow. $T_{\rm d5\%}$ is defined as temperature at which 5% weight loss of the polymer sample was observed. A TA Instruments Q800 dynamic mechanical analyzer (DMA) in film tension mode with a single frequency of 1 Hz at a heating rate of 5 °C/min was employed to determine the mechanical properties of the network films. DMA experiments were completed in duplicate and the values reported are from the second heating event. The influence of water absorption, as a result of the sample being conditioned in the humidity chamber, was examined. Three samples of each PIL were placed into an Espec BTL-433 benchtop temperature/humidity oven, set to 30 °C and the desired relative humidity (30, 50 or 70%). To simulate 100% relative humidity conditions, samples were instead submerged in a vial containing DI water. Each sample was weighed prior to the experiment (m_{drv}) and then placed into the humidity chamber (or submerged in DI water) where it was conditioned for 16 h. The sample was then removed, blotted with a paper towel to remove any surface moisture and weighed (m_{wet}). Water absorption was determined using the following equation: water absorbed (%) = $((m_{\text{wet}}-m_{\text{dry}})/m_{\text{dry}}) \times 100$. An average error of 0.08% was determined across all % water absorbed measurements.

2.2. Conductivity measurements

For experiments under anhydrous conditions, a TA Instruments DHR-2 Discovery Hybrid Rheometer with dielectric accessory and Keysight Technologies E4980AL/120 LCR meter was utilized. A sample with approximate thickness of 500 μ m was placed between the two 25 mm stainless steel, parallel plate electrodes of the dielectric accessory and the environmental chamber, under an atmosphere of dry nitrogen and cooled with liquid nitrogen, was closed. Dielectric permittivity and

conductivity were measured isothermally with an ac amplitude of ± 0.01 V in 10 °C steps over a frequency range of 20.0–10⁶ Hz. Samples were kept at a constant axial force of 5.0 ± 0.2 N and allowed to soak at each temperature for 45 min prior to obtaining measurements. For variable humidity experiments, DRS measurements were performed using an in-house, custom-built, two-electrode cell coupled to a Metrohm Autolab 302 N potentiostat and FRA32 M frequency response analyzer [37]. Circular disks (12 mm diameter) were cut from each ionene film (500 μm thickness) and placed between the two stainless steel electrodes of the cell. The cell was placed inside a controlled-temperature/humidity chamber (Espec BTU-433), set to the desired relative humidity (30, 50 or 70%). Dielectric permittivity and conductivity were measured isothermally over a frequency range of $0.1-10^7$ Hz with an ac amplitude of ± 0.01 V in 10 °C steps. Samples were soaked at each individual temperature until a constant conductivity was observed (45–50 min). The DC-conductivity (σ_{DC}) was determined from the plateau value observed in the frequency-dependent spectrum of the real component of the complex conductivity ($\sigma' = \omega \epsilon'' \epsilon_0$ where ω is the frequency, ε'' is the dielectric loss and ε_0 is the vacuum permittivity).

3. Results and discussion

The desired imidazolium-containing ene monomers were prepared as outlined in Scheme 1. In short, substitution of sodium imidazole with 6-iodohexene resulted in 1-(hex-5-enyl)imidazole 1. Quaternization was then accomplished by reaction of 1 with 6-chlorohexene, providing 1,3-bishexenylimidazolium chloride 2a. Standard anion metathesis reactions were then completed with the appropriate lithium, sodium or silver salt, providing ene monomers 2b-g. Structural characterization and purity of the IL monomers and intermediates were determined using $^1\mathrm{H}$ and $^{13}\mathrm{C}$ NMR spectroscopy and elemental analysis. Residual chloride was determined to be <0.01% w/w in monomers 2b-g by ion chromatography.

Differential scanning calorimetry (DSC) was utilized to determine the thermal transitions of IL ene monomers 2a-g (Table S1). As expected, the glass transition temperatures (T_g) of the monomers decreased with increasing size of the counteranions (based upon thermochemical radii) as follows: [OMs] \approx [PF6] < [ClO4] < [NO3] < [Cl] [46,47]. T_g values for monomers with the largest anions [NTf2] and [OTf] were below the lower limit of the instrumentation (<-90 °C). Thermal stability, as defined by $T_{d5\%}$ (the temperature at which 5% weight loss was observed), was analyzed by thermgravimetric analysis (TGA) and values were found to decrease with increasing Lewis basicity of the counteranions on the order of [NTf2] > [PF6] > [OTf] > [ClO4] > [OMs] > [NO3] > [Cl]. Such a correlation between Lewis basicity and thermal stability has been well established for imidazolium ILs and IL-functionalized polymers by our group and others [38,48–51].

Thiol-ene photopolymerization (Scheme 1) was completed using a

broad-band UV source utilizing PTMP as the multi-functional thiol and TPO as the photoiniator (1 wt%). The thiol:ene functional group ratio was kept stoichiometric for all polymerizations. For each experiment, the monomer solution was dispensed by syringe between two Rain-X® treated glass slides, separated by a 500 μm PTFE spacer and held together by binder clips. The solution was polymerized under the UV lamp on each side for 5 min. The resulting ionene films were then placed in a vacuum oven overnight to dry. The films were found to be insoluble in a number of conventional solvents, including water, acetone, chloroform, dimethylsulfoxide, tetrahydrofuran, methanol and N,N-dimethylformamide.

As with the monomers, the ionene networks were analyzed for their thermal properties using DSC and TGA (Table 1). Glass transition temperatures once again were found to decrease with increasing counteranion size on the order of [NTf₂] < [OTf] < [OMs] < [PF₆] < [ClO₄] < [NO₃] < [Cl] (Fig. S19). All ionenes exhibited $T_{\rm g}$ values higher than the corresponding IL monomers due to covalent integration into the polymer network. Overall, the networks were found to have higher $T_{\rm d5\%}$ values than their monomeric precursors, especially for the more Lewis basic anions such as chloride, nitrate and mesylate (Fig. S20).

Soxlhet extraction in THF revealed very high gel fractions (>95.5%) across all of the ionene networks, indicating a high degree of network formation (Table 1). This notion was supported by FT-IR spectroscopy, where no detectable thiol (2570 cm⁻¹) or alkene (1630 cm⁻¹) bands were observed (detection limit/error of 2%) after photopolymerization. None of the networks were found to swell to a high extent in THF, although a slight increase in the ability to swell does appear to occur as the anion gets larger and the network more hydrophobic (for example [OTf], [PF₆] and [NTf₂]). This observation is attributed to an enhancement in polymer-solvent interactions as the network becomes more hydrophobic.

The range of observed rubbery plateau moduli (E' at 100 °C), as determined by dynamic mechanical analysis of the networks, was relatively narrow (5.7–7.5 MPa), which was not surprising since the thiol: ene functional group ratio was stoichiometric for all formulations (Fig. 1). Apparent crosslink densities (ρ_x) were calculated according to rubbery elasticity theory ($\rho_x = E'/3$ RT) and were found to be in the range of 6.2–8.0 \times 10⁻⁴ mol/cm³ (Table 1) [45]. DMA T_g values, determined from the maximum of the tan δ curves (Fig. S21), indicated that, as with the DSC data, the counteranion size heavily influenced the T_g . The order ([NTf₂] < [OTf] < [OMs] < [ClO₄] < [NO₃] < [PF₆] < [Cl]) was slightly different than what was observed by DSC, however it is worth noting that many of the mid-sized anions ([ClO₄], [NO₃], [PF₆]) have similar thermomechanical radii [46,47].

Temperature-dependent ionic conductivites of the ionene networks were initially determined under anhydrous conditions utilizing a TA Instruments DHR-2 Rheometer equipped with the dielectric accessory. At lower temperatures (Fig. 2), ionic conductivity was found to have an inverse relationship with $T_{\rm g}$, presumably due to the existence of the

Scheme 1. Synthesis of covalently crosslinked ionene networks, prepared from 1,3-bishexenylimidazolium IL ene monomers 2a-g.

Table 1Gel fraction, thermal and mechanical properties of the imidazolium-containing ionene networks.

Network	Gel fraction (%)	% swelling	DSC T_g (°C)	TGA $T_{d5\%}$ (°C)	$\it E'$ @ 100 °C (MPa)	tan δ max (°C)	$ ho_{\rm x} \ { m x} \ { m 10}^{-4} \ ({ m mol/cm}^3)$
Cl	98.0 ± 0.3	122 ± 4	11.6	284	$\textbf{7.48} \pm \textbf{0.13}$	36.9 ± 0.2	8.04 ± 0.1
NO_3	97.7 ± 0.2	123 ± 2	5.4	287	5.85 ± 0.12	19.2 ± 0.3	6.29 ± 0.1
OMs	99.5 ± 0.2	125 ± 3	-9.0	328	6.89 ± 0.15	17.1 ± 0.2	7.40 ± 0.2
OTf	99.1 ± 0.2	136 ± 2	-9.5	342	6.58 ± 0.21	9.4 ± 0.2	7.07 ± 0.2
PF_6	95.5 ± 0.4	136 ± 3	1.7	346	6.91 ± 0.24	24.3 ± 0.3	$\textbf{7.42} \pm \textbf{0.3}$
ClO ₄	99.6 ± 0.1	125 ± 3	4.4	336	6.05 ± 0.18	21.7 ± 0.1	6.50 ± 0.2
NTf ₂	97.2 ± 0.3	154 ± 3	-12.7	364	5.78 ± 0.14	2.8 ± 0.2	6.21 ± 0.1

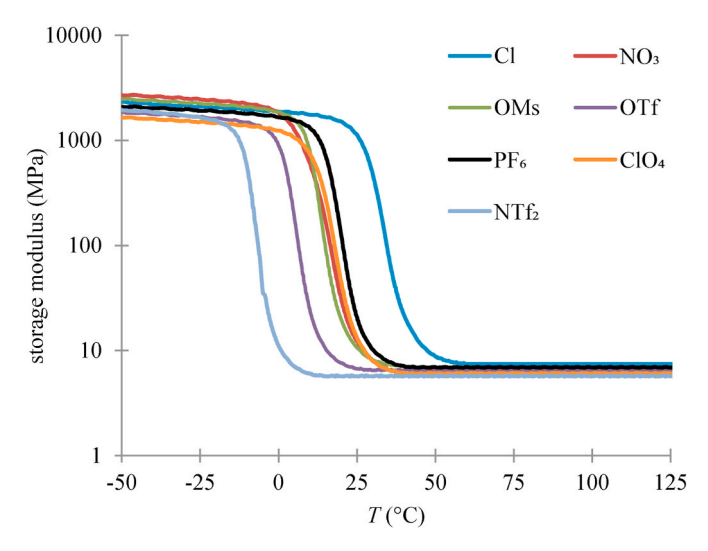


Fig. 1. Overlay of temperature-dependent storage modulus (E') data from dynamic mechanical analysis.

weaker ionic association and plasticizing effect that commonly occur with larger anions such as [OTf] and [NTf₂]. Overall, ionic conductivity at 20 °C was found to increase on the order of: [Cl] < [NO₃] < [PF₆] < [ClO₄] < [OMs] < [OTf] < [NTf₂] with a range encompassing four orders of magnitude (10 $^{-6}$ to 10 $^{-10}$ S/cm).

The anhydrous ionic conductivity curves were fitted to the Vogel-Fulcher-Tamman (VFT) equation:

$$\sigma(T) = \sigma_{\infty} \times \exp(\frac{-DT_o}{T - T_o}) \tag{1}$$

where σ_{∞} is the infinite conductivity limit, D is the strength parameter, T_{o} is the Vogel temperature (the temperature in which ion mobility goes to zero and polymer relaxation time is infinite) and T is the experimental

temperature [39,52,53]. The results from the fitting are represented as dashed lines in the plot of anhydrous conductivity in Fig. 2 and the VFT fitting parameters are provided in Table 2. High temperature limiting conductivities (σ_{∞}) were found to correlate within reason with the thermochemical radii of the corresponding counteranions, (i.e. σ_{∞} increased with decreasing anion size). The network bearing the Cl counteranion exhibited the highest σ_{∞} while the network employing the NTf_2 counteranion exhibited the lowest σ_{∞} , representing the two extremes. Since anion size appears to be a correlating factor, this observation likely results from the smaller, more basic anions overcoming electrostatic/Coulombic barriers as temperature increases. In a recent study, it has been demonstrated that conductivity of ionic polymers containing smaller ions is mostly controlled by such electrostatic interactions, while conductivities in polymers with larger, less basic anions are impacted strongly by elastic energy barriers (i.e. polymer free volume or mesh size) [54]. In the networks of present concern, it is possible that elastic barriers to ion motion are relatively small, and change very little, across a wide range of temperatures owing to the size of the spacer groups and the crosslinked nature of the polymers. At the same time, it is also likely that, due to the wide variety of sizes and geometries of the mobile counteranions, that there are differences in ion aggregation, both in extent and structure, that are impacting conductivities [55]; however, additional morphological and/or computational studies would be required to support this hypothesis.

 $T-T_0$ values were found to be comparable to our previously reported thiol-ene network data [39] but slightly higher than what have been observed for other imidazolium PILs [36,56–58]. The strength parameter D, which is inversely related to dynamic fragility, was found to generally increase with decreasing counteranion size, although the majority of the ionene networks (except [Cl] and [NTf2]) exhibited similar values (± 0.7 units). Larger D values have been associated with more Arrhenius-like behavior and increased coupling between free ion motion and polymer chain dynamics [39,52,53].

Ionic conductivity as a function of normalized $T_{\rm g}$ was also investigated in an effort to suppress the influence of changes in ionomer $T_{\rm g}$ and polymer segmental dynamics (Fig. 2). As the $T_{\rm g}$ -normalized curves do

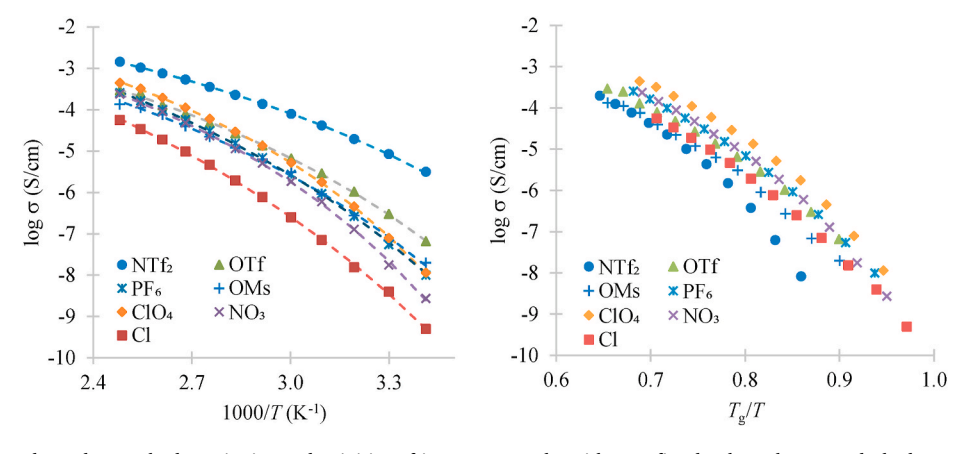


Fig. 2. (Left) Temperature-dependent, anhydrous ionic conductivities of ionene networks with VFT fitted values shown as dashed curves for the anhydrous conductivity data. (Right) T_g -normalized ionic conductivities of the ionene networks shows that differences in ionic conductivity are not solely related to changes in T_g .

Table 2VFT Fitting, ion concentration and mobility data parameters for the ionene networks.

Network	σ at 20 °C (S/cm)	$\sigma_{\infty}(S/cm)$	D	$T_g - T_o$ (K)	$\log \mu_{\infty}$ $(cm^2$ V^{-1} $s^{-1})$	E _a (kJ mol ⁻¹)	$\log p_{\infty}$ (cm ⁻³)
Cl	5.0×10^{-10}	8.09	14.3	93	-0.17	20.13	19.6
NO_3	$\begin{array}{c} 3.0 \times \\ 10^{-9} \end{array}$	1.09	7.6	67	-0.08	22.74	19.7
OMs	$\begin{array}{c} 2.0 \times \\ 10^{-8} \end{array}$	0.61	8.9	78	0.02	22.16	19.6
OTf	$^{6.6\times}_{10^{-8}}$	0.64	8.3	82	0.41	15.29	18.8
PF ₆	$1.0\times\\10^{-8}$	4.13	11.0	70	0.77	10.30	18.2
ClO ₄	$1.1\times\\10^{-8}$	3.56	9.0	71	0.70	11.62	18.7
NTf ₂	$\begin{array}{c} 1.5\times\\10^{-6}\end{array}$	0.32	6.6	69	0.95	8.25	18.1

not converge well the observed differences in ionic conductivity cannot be solely related to changes in $T_{\rm g}$. As previously alluded to, the interplay between morphology, molecular structure and ionic conductivity can be very complex and further experimentation would be necessary in order to completely separate these interconnected parameters.

However, elucidating the relative contributions of free-ion concentration (p), free-ion mobility (μ) , and polymer segmental dynamics to conductivity under anhydrous conditions could provide some initial insight into polymer characteristics controlling conductivities. Thus, the obtained dielectric data was evaluated by fitting both ε' and ε'' with previously reported models, the details of which are provided in the Supporting Information (Fig. S22). More specifically, the Debye-type relaxation function of modified Macdonald's theory was applied to the low-frequency electrode polarization regime of both spectra. At the same time, information about polymer relaxations was extracted from the higher-frequency part of the spectra by fitting with a Havriliak-Negami function [39,52,59–61]. The dependence of free-ion concentration (number density of conducting ions) on temperature can be fitted to an Arrhenius function:

$$p = p_{\infty} \times exp(\frac{-E_a}{RT}) \tag{2}$$

where p_{∞} is the high-temperature free-ion concentration limit and E_a is the activation energy for ion pair dissociation (Fig. 3) [39,61]. From the fitted lines, it was determined that $\log p_{\infty}$ values for the ionene networks were in the range of $19.0 \pm 0.7~{\rm cm}^{-3}$ and were lower than the estimated values of $\sim\!21~{\rm cm}^{-3}$ calculated from monomer stoichiometries (Table 2), meaning they are generally less "free" to participate in conduction than predicted. Activation energies were found to correlate with ion binding ability (Lewis basicity or hydrogen bond accepting capability) as expected (Fig. S23) [50]. The stronger the ion binding affinity (chloride for example), the large the amount of energy needed for the ion to dissociate from any ion pairs or clusters. This result is consistent with the idea that temperature-dependent conductivites depend, at least in part, on electrostatic barriers to ion motion.

Temperature-dependent ion mobilites were found by using a VFT fitting similar to that used for ionic conductivities:

$$\mu(T) = \mu_{\infty} \times exp(\frac{-D T_o}{T - T_o}) \tag{3}$$

where μ_{∞} represents the high-temperature ion mobility limit and other parameters defined as before (Fig. 4). Ion mobility was found to be inversely related to Lewis basicity. Ionenes employing stronger Lewis bases ([Cl], [NO₃], [OMs]) exhibited lower mobility values than the weaker, non-coordinating bases ([PF₆], [ClO₄], [OTf], [NTf₂]). These

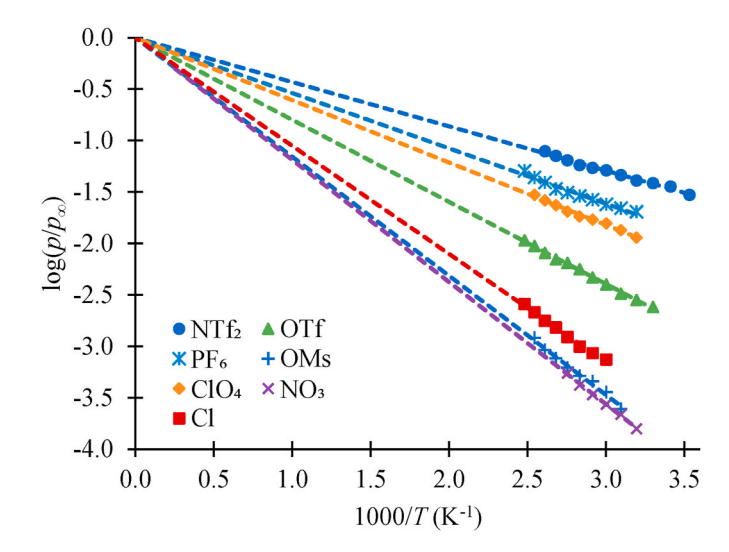


Fig. 3. Temperature-dependent free ion concentrations determined by fitting dielectric spectra with the modified Macdonald model. The dashed lines represent the linear Arrhenius fits extrapolated to the complete dissociation limit.

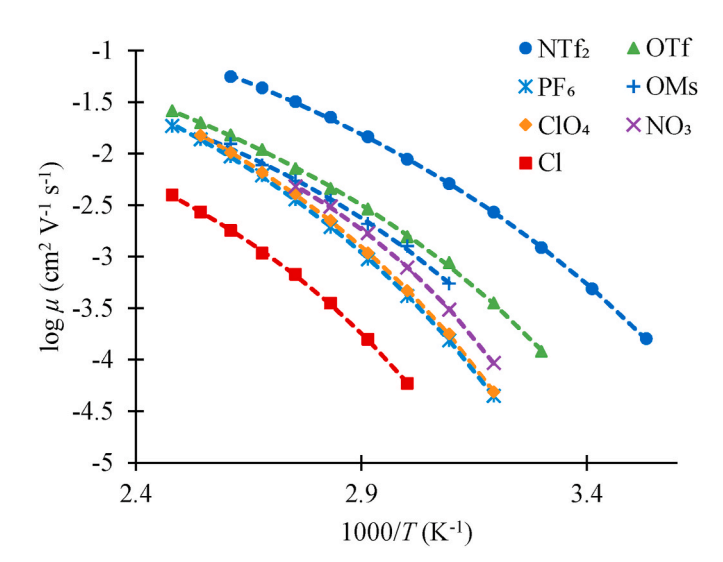


Fig. 4. Temperature-dependent free ion mobilities determined by fitting dielectric spectra with the modified Macdonald model. The dashed curves represent the VFT fits.

results match well with the order of ionene conductivity over the same temperature range. What is somewhat surprising is that, despite having the highest limiting conductivity, chloride exhibits the smallest limiting mobility (μ_{∞}) . The reverse is true for [NTf₂], which had the lowest limiting conductivity but the greatest limiting mobility. It should be noted, however, that the limiting mobilities also follow a general trend with anion/network hydrophobicity (as expressed by free energy of phase transfer between organic and aqueous phases) [62]. One hypothesis, then, for the observed mobility/conductivity trends is based on the idea of percolated aggregate theory [55]. Larger, more non-coordinated anions (more hydrophobic networks) may exist within a network of interconnected ionic aggregates, across all temperatures, which facilitate free ion motion (e.g., anion hopping) throughout the material. On the other hand, the smaller, more basic, ions (more hydrophilic networks) may reside primarily within smaller ionic clusters, perhaps even as small as ion pairs, within the material. Due to anion size and tighter cation-anion contact, there is likely to be very little interconnection between such ion pairs/clusters regardless of temperature,

thereby restricting the mobility of the smaller anions.

This hypothesis alone, though, does not fully explain why the limiting mobilities and limiting conductivities do not correspond neatly with one another. As noted earlier, the limiting free ion concentrations for the various ionenes generally were within an order of magnitude of one another. However, closer inspection of the log p_{∞} values show that there is a trend of increasing $log p_{\infty}$ that also correlates with increasing anion basicity and network hydrophilicity, i.e, in the opposite direction of the limiting mobility trend. So, it appears that the amount of free ion contributing to conductivity increases much more rapidly/greatly for smaller, more basic anions (hydrophilic networks) than it does with larger, non-coordinating anions (hydrophobic networks). This observation is likely due, again, to the possible differences in morphologies among the polymers outlined above. For instance, as temperature increases, anions in percolated aggregate networks generally remain contained within such aggregates (though those aggregates may become somewhat more diffuse) and total "free" anions remain rather low. Such observations with other ionic polymer systems have been recently reported [55]. On the other hand, once sufficient thermal energy is input to overcome electrostatic interactions present for smaller, basic anions a large number of those ions become free to contribute to conductivity (though those ions' mobilities may be limited for reasons outlined above). In other words, while these ionenes all have nominally \sim the same total anion concentration, they are behaving as if they have very different anion loading due to variations in ion cluster/aggregation morphologies. Of course, in order to fully support these assertions, X-ray scattering studies will be required.

As alluded to earlier, ionic conductivity can vary greatly with humidity and water absorption. Towards this end, temperature-dependent ionic conductivities were determined using dielectric relaxation spectroscopy (DRS) where the relative humidity was controlled at 30, 50 or 70% (Fig. 5). As expected, the polymer employing the chloride ion (most hydrophilic network) exhibited a tremendous enhancement (~5 orders

of magnitude at 30 °C, 70% RH) in ionic conductivity with increasing humidity. Networks using either the $[NO_3]$ or [OMs] anion were also found to exhibit large enhancements in conductivity with increasing humidity. Hydrophobic networks which used anions such as $[ClO_4]$, [OTf], $[PF_6]$ and $[NTf_2]$ showed little to no difference regardless of the conditions. Overlays of temperature-dependent ionic conductivity curves, as a function of relative humidity, for individual networks can be found in the Supporting Information (Figs. S24-S30).

To supplement these findings, each network was subjected to water uptake studies at the relative humidity of interest (30, 50 or 70%), as well as after a 16 h soaking in water to mimic 100% relative humidity, to determine the percent of water absorbed (Fig. 6). Water uptake was found to be the largest for chloride system as expected, however the mesylate-containing network was also observed to have a relatively large water uptake. Hydrophobic networks ([PF₆] and [NTf₂]) did not absorb any appreciable water at any humidity studied. It is also worth noting that water uptake was found to be consistent across the 30-90 °C temperature range. Overall, the results from these studies mirror those acquired from ionic conductivity studies. Clearly, the more hydrophilic the network is, the more water is absorbed, resulting in a system where ion transport is less dependent upon polymer chain dynamics (NafionTMlike). It is hypothesized that, similar to the PIL systems described by Elabd and Madsen, increased water content is assisting in the formation of ion channels within the network which, in turn, enhances ion transport [27,52,63]. The T_g values of the ionene networks were also monitored as a function of relative humidity. In each experiment, a sample of the film was taken directly out of the humidity-controlled oven and placed in a hermetically sealed aluminum pan, followed by analysis using DSC. Fig. 6 includes the results of these experiments which nicely complement the ionic conductivity and water uptake trends. Networks employing hydrophilic anions [Cl], [OMs] or [NO₃] exhibited drastic decreases in T_g as a function of relative humidity while [PF₆] and [NTf₂] were unchanged. T_g -Normalization graphs at variable relative humidity

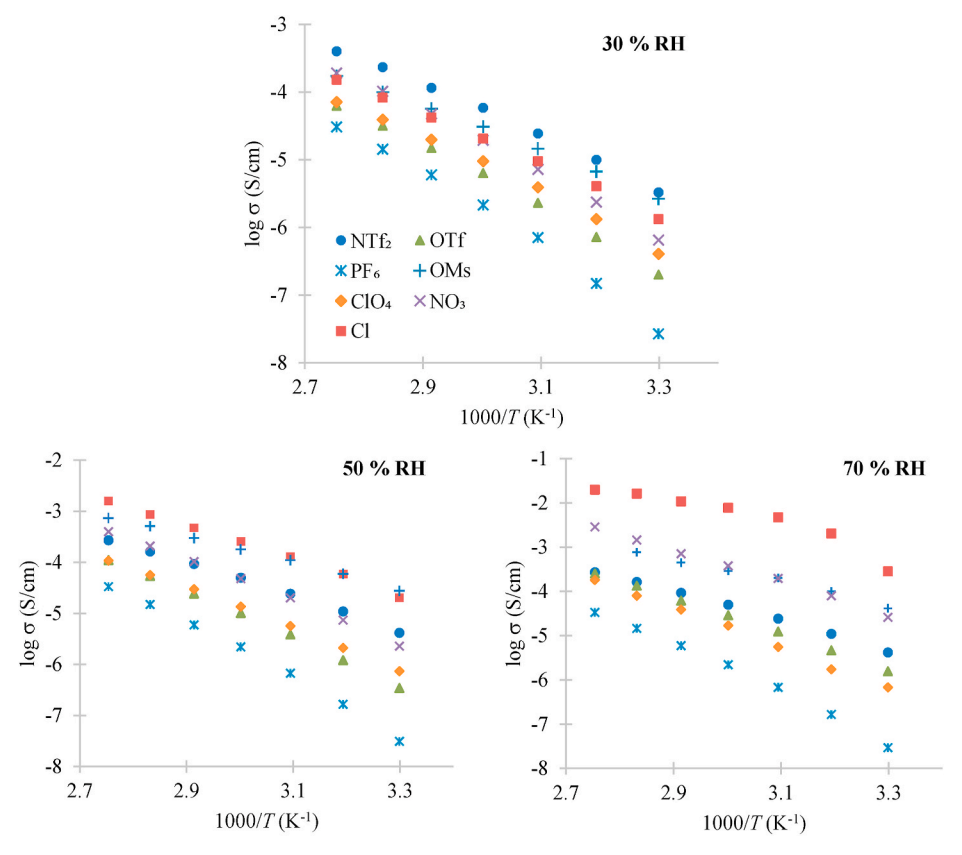
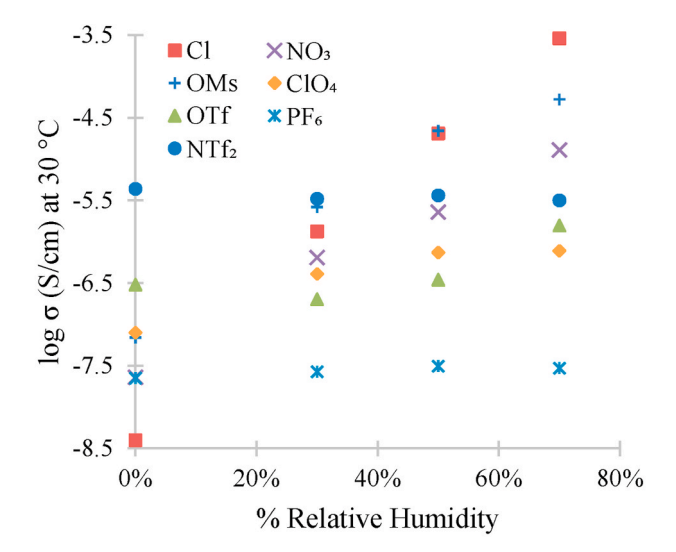
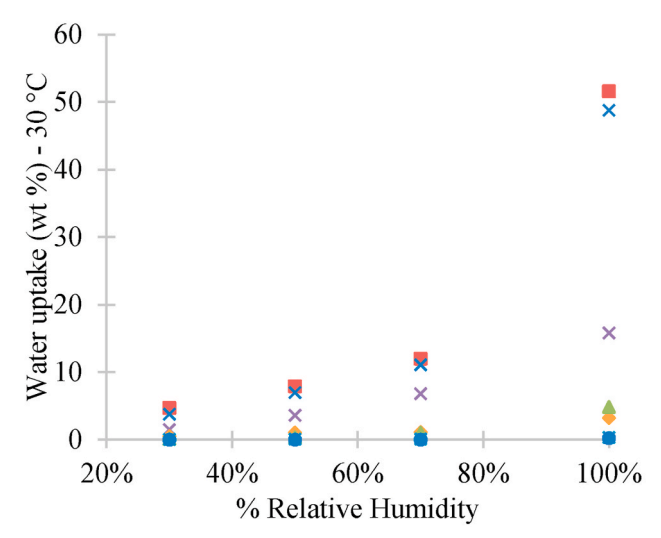


Fig. 5. Temperature-dependent ionic conductivities of ionene networks under different relative humidity conditions.





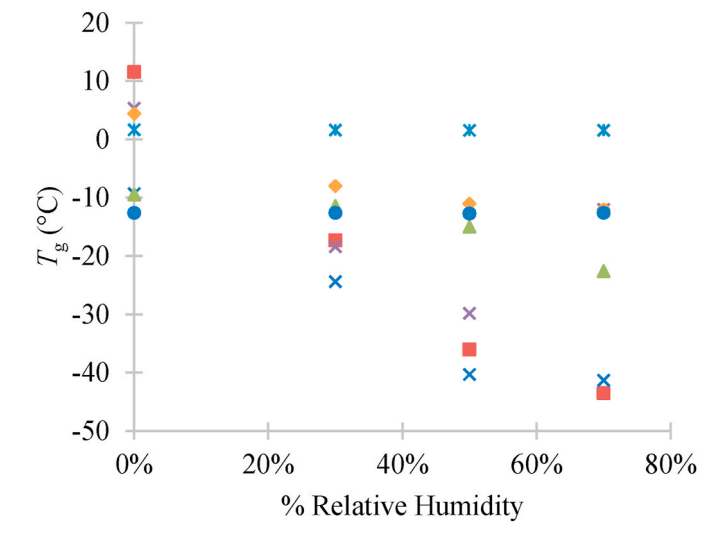


Fig. 6. Influence of relative humidity at 30 $^{\circ}$ C on ionic conductivity (top), water uptake (middle) and glass transition temperature(bottom). The legend for all three comparisons is located in the graph on the top.

were assembled in an attempt to decipher the role that $T_{\rm g}/{\rm polymer}$ dynamics have on the observed changes in ionic conductivity (Fig. S31). A complete coelescnce of the networks most effected by humidity ([CI], [NO₃], [OMs]) was not observed, indicating that the observed increase in conductivity is not solely a $T_{\rm g}$ phenomenon. For two networks that were moderately affected by an increase in humidity ([OTf], [ClO₄]), the $T_{\rm g}$ -normalized curves were found to coalesce, indicating that water may be primarily acting to plasticize the network as reflected in a reduction in $T_{\rm g}$.

4. Summary

The influence of counteranion and humidity on the thermal and mechanical properties and ionic conductivities of a series of covalently crosslinked ionenes was investigated. Thiol-ene photochemistry was utilized to prepare the desired networks with PTMP as a tetrafunctional thiol and a wide range of counteranions ([NTf₂], [PF₆], [OTf], [ClO₄], [OMs], [NO₃], [Cl]) were included as part of the design of experiment. All of the networks exhibited a relatively high crosslink density (E′ of 5.8–7.5 MPa at 100 °C), with $T_{\rm g}$ values found to be inversely related to the size of the counteranion. Thermal stability ($T_{\rm d5\%}$) was inversely related to the Lewis basicity of the counteranions with the ionene network bearing the [NTf₂] anion exhibiting the highest thermal stability (>360 °C).

Anhydrous ionic conductivities, as determined from dielectric relaxation spectroscopy, were found to be on the order of 10^{-10} to 10^{-6} S/cm at 20 °C. At lower temperatures, ionic conductivity was found to have an inverse relationship with T_g as larger, non-coordinating anions such as [OTf] and [NTf2] result in weaker ionic associations and plasticize the network. VFT fitting of the anhydrous conductivity curves indicated that high temperature limiting conductivities (σ_{∞}) were found to correlate within reason with the thermochemical radii of the corresponding counteranions with the Cl-bearing network exhibiting the highest σ_{∞} value. Although further morphological and/or computational studies are needed, this data could be indicative of differences in ion aggregation, both in extent and structure. The relative contributions of free-ion concentration (p), free-ion mobility (μ), and polymer segmental dynamics to conductivity under anhydrous conditions was also investigated. Ionenes employing weaker, non-coordinating bases ([PF₆], [ClO₄], [NTf₂]) exhibited higher mobility values than stronger Lewis bases ([Cl], [NO₃], [OMs]) and could be attributed to the existence of more interconnected network ionic aggregates across all temperatures. Smaller, more basic ions (more hydrophilic networks) may reside primarily within smaller ionic clusters with little interconnection and restricted mobility. Free ion concentration was found to increase much more rapidly/greatly for these anions and may reflect that these percolated aggregates may be more diffuse throughout the network; however additional morphological studies would need to be carried out.

Finally, the effect of relative humidity on the ionic conductivity of the ionene networks was also explored. The most hydrophilic networks ([Cl], [OMs], [NO₃]) were found to have a very large response to humidity changes, resulting in a 3- to 5-fold enhancement in conductivity. Water tends to have a plasticizing effect in most ion-containing networks, leading to a decrease in $T_{\rm g}$ and an increase in conductivity; however, as the $T_{\rm g}$ -normalized curves did not completely collapse, the rate enhancement cannot be completely related to polymer chain dynamics. As has been suggested in related publications, a water-assisted ion transport mechanism can be envisioned for these networks. Additional morphological studies on these systems (anhydrous and under controlled humidity) are planned as part of a follow-on study.

Declaration of competing interest

The authors declare that they have no known competing financial interests or personal relationships that could have appeared to influence the work reported in this paper.

Acknowledgements

This work was supported by a Research in Undergraduate Institutions (RUI) award from the National Science Foundation, Division of Materials Research, Polymers Program (DMR-1708632). Thermal and mechanical analyses were conducted in the Polymer and Materials Science Laboratory (PMCL) at Murray State University. Financial support for the DMA and rheometer was provided by the National Science Foundation (Major Research Instrumentation) under DMR-1427778 and DMR-1828251, respectively.

Appendix A. Supplementary data

Supplementary data to this article can be found online at https://doi.org/10.1016/j.polymer.2021.123641.

References

- D. Mecerreyes, Polymeric ionic liquids: broadening the properties and applications of polyelectrolytes, Prog. Polym. Sci. 36 (2011) 1629–1648.
- [2] J. Yuan, D. Mecerreyes, M. Antonietti, Poly(ionic liquid)s: an update, Prog. Polym. Sci. 38 (2013) 1009–1036.
- [3] W. Qian, J. Texter, F. Yan, Frontiers in poly(ionic liquid)s: syntheses and applications, Chem. Soc. Rev. 46 (2017) 1124–1159.
- [4] S. Williams, T.E. Long, Recent advances in the synthesis and structure-property relationships of ammonium ionenes, Prog. Polym. Sci. 34 (2009) 762–782.
- [5] J.E. Bara, K.E. O'Harra, Recent advances in the design of ionenes: towards convergence with high-performance polymers, Macromol. Chem. Phys. 220 (2019) 1900078.
- [6] M. Guo, J. Fang, H. Xu, W. Li, X. Lu, C. Lan, K. Li, Synthesis and characterization of novel anion exchange membranes based on imidazolium-type ionic liquid for alkaline fuel cells, J. Membr. Sci. 362 (2010) 97.
- [7] O.D. Thomas, K.J.W.Y. Soo, T.J. Peckham, M.P. Kulkarni, S. Holdcroft, Anion conducting poly(dialkyl benzimidazolium) salts, Polym. Chem. 2 (2011) 1641.
- [8] Y. Ye, Y.A. Elabd, Relative chemical stability of imidazolium-based alkaline anion exchange polymerized ionic liquids, Macromolecules 44 (2011) 8494–8503.
- [9] N.J. Robertson, H.A. Kostalik IV, T.J. Clark, P.F. Mutolo, H.D. Abruña, G.W. Coates, Tunable high performance cross-linked alkaline anion exchange membranes, J. Am. Chem. Soc. 132 (2010) 3400–3404.
- [10] B. Lin, L. Qiu, B. Qiu, Y. Peng, F. Yan, A soluble and conductive polyfluorene ionomer with pendant imidazolium groups for alkaline fuel cell applications, Macromolecules 44 (2011) 9642–9649.
- [11] O.D. Thomas, K.J.W.Y. Soo, T.J. Peckham, M.P. Kulkarni, S. Holdcroft, A stable hydroxide-conducting polymer, J. Am. Chem. Soc. 134 (2012) 10753.
- [12] J.R. Nykaza, Y. Ye, R.L. Nelson, A.C. Jackson, F.L. Beyer, E.M. Davis, K. Page, S. Sharick, K.I. Winey, Y.A. Elabd, Polymerized ionic liquid diblock copolymers: impact of water/ion clustering on ion conductivity, Soft Matter 12 (2016) 1132-1144
- [13] P. Cotanda, N. Petzetakis, X. Jiang, G. Stone, M.P. Balsara, Hydroxide-ion transport and stability of diblock copolymers with a polyallyldimethyl ammonium hydroxide block, J. Polym. Sci. 55 (2017) 2243–2248.
- [14] S. Zulfigar, M.I. Sarwar, D. Mecerreyes, Polymeric ionic liquids for CO2 capture and separation: potential, progress and challenges, Polym. Chem. 6 (2015) 6435–6451.
- [15] Z. Dai, R.D. Noble, D.L. Gin, X. Zhang, L. Deng, Combination of ionic liquids with membrane technology: a new approach for CO₂ separation, J. Membr. Sci. 497 (2016) 1–20.
- [16] M.G. Cowan, D.L. Gin, R.D. Noble, Poly(ionic liquid)/ionic liquid ion-gels with high "free" ionic liquid content: platform materials for CO₂/light gas separations, Acc. Chem. Res. 49 (2016) 724–732.
- [17] A.S. Shaplov, S.M. Morozova, E.I. Lozinskaya, P.S. Vlasov, A.S.L. Gouveia, L. C. Tome, I.M. Murrucho, Y.S. Vygodskii, Turning into poly(ionic liquid)s as a tool for polyimide modification: synthesis, characterization and CO2 separation properties, Polym. Chem. 7 (2016) 580.
- [18] M.S. Mittenthal, B.S. Flowers, J.E. Bara, J.W. Whitley, S.K. Spear, J.D. Roveda, D. A. Wallace, M.S. Shannon, R. Holler, R. Martens, D.T. Daly, Ionic polyimides: hybrid polymer architectures and composites with ionic liquids for advanced gas separation membranes, Ind. Eng. Chem. Res. 56 (2017) 5055.
- [19] K. E. O'Harra, I. Kammakakam, D. M. Noll, E. M. Turfinger, G. P. Dennis, E. M. Jackson, J. E. Bara. Synthesis and performance of aromatic polyamide ionenes as gas separation membranes. Membranes 10 (2020), 51-66.
- [20] T.P. Lodge, A unique platform for materials design, Science 312 (2008) 50-51.
- [21] T.P. Lodge, T. Ueki, Mechanically tunable, readily processable ion gels by self-assembly of block copolymers in ionic liquids, Acc. Chem. Res. 49 (2016) 2107–2114.
- [22] E. Margaretta, G.B. Fahs, D.L. Inglefield, C. Jangu, D. Wang, J.R. Heflin, R. B. Moore, T.> E. Long, Imdazolium-containing ABA triblock copolymers as electroactive devices, ACS Appl. Mater. Interfaces 8 (2016) 1280–1288.
- [23] G.J. Turdyn, W. Liu, S.-W. Wang, R.H. Colby, Counterion dynamic in polyestersulfonate ionomers with ionic liquid counterions, Macromolecules 44 (2011) 3572–3582.

[24] M.A. Hickner, Water-mediated transport in ion-containing polymers, J. Polym. Sci., Part B: Polym. Phys. 50 (2012) 9–20.

- [25] K.M. Meek, S. Sharick, Y. Ye, K.I. Winey, Y.A. Elabd, Bromide and hydroxide conductivity-morphology relationships in polymerized ionic liquid block copolymers, Macromolecules 48 (2015) 4850–4862.
- [26] K.A. Mauritz, R.B. Moore, State of understanding of nafion, Chem. Rev. 104 (2004) 4535–4585.
- [27] L.M. Thieu, L. Zhu, A.G. Korovich, M.A. Hickner, L.A. Madsen, Multiscale tortuous diffusion in anion and cation exchange membranes, Macromolecules 52 (2019) 24–35.
- [28] S.R. Williams, D. Salas-de la Cruz, K.I. Winey, T.E. Long, Ionene segmented block copolymers containing imidazolium cations: structure-property relationships as a function of hard segment content, Polymer 51 (2010) 1252–1257.
- [29] S.R. Williams, W. Wang, K.I. Winey, T.E. Long, Synthesis and morphology of segmented poly(tetramethylene oxide)-based polyurethanes containing phosphonium salts, Macromolecules 41 (2008) 9072–9079.
- [30] R. Gao, M. Zhang, S. Wang, R.B. Moore, R.H. Colby, T.E. Long, Polyurethanes containing an imidazolium diol-based ionic-liquid chain extender for incorporation of ionic-liquid electrolytes, Macromol. Chem. Phys. 214 (2013) 1027–1036.
- [31] M. Lee, U.H. Choi, D. Salas-de la Cruz, A. Mittal, K.I. Winey, R.H. Colby, H. W. Gibson, Imidazolium Polyesters, Structure-Property relationships in thermal behavior, ionic conductivity, and morphology, Adv. Fucnt. Mater. 21 (2011) 708–717.
- [32] C.M. Evans, C.R. Bridges, G.E. Sanoja, J. Bartels, R.A. Segalman, Role of tethered ion placement on polymerized ionic liquid structure and conductivity: pendant versus backbone charge placement, ACS Macro Lett. 5 (2016) 925–930.
- [33] L.M. Hall, M.E. Seitz, K.I. Winey, K.L. Opper, K.B. Wagener, M.J. Stevens, A. L. Frischknecht, Ionic aggregate structure in ionomer melts: effect of molecular architecture on aggregates and the ionomer peak, J. Am. Chem. Soc. 134 (2012) 574–587.
- [34] L.M. Hall, M.J. Stevens, A.L. Frischknecht, Dynamics of model ionomer melts of various architectures, Macromolecules 45 (2012) 8097–8108.
- [35] C.L. Ting, M.J. Stevens, A.L. Frischknecht, Structure and dynamics of coarse-grained ionomer melts in an external electric field, Macromolecules 48 (2015) 809–818.
- [36] Q. Zhao, C. Shen, K.P. Halloran, C.M. Evans, Effect of network architecture and linker polarity on ion aggregation and conductivity in precise polymerized ionic liquids, ACS Macro Lett. 8 (2019) 658–663.
- [37] A. Nguyen, T.C. Rhoades, R.D. Johnson, K.M. Miller, Influence of anion and crosslink density on the ionic conductivity of 1,2,3-triazolium-based poly(ionic liquid) polyester networks, Macromol. Chem. Phys. 218 (2017) 1700337.
- [38] C.A. Tracy, A.M. Adler, A. Nguyen, R.D. Johnson, K.M. Miller, Covalently crosslinked 1,2,3-triazolium-containing polyester networks: thermal, mechanical and conductive properties, ACS Omega 3 (2018) 13442–13453.
- [39] T.C. Rhoades, J.C. Wistrom, R.D. Johnson, K.M. Miller, Thermal, mechanical and conductive properties of imidazolium-containing thiol-ene poly(ionic liquid) networks, Polymer 100 (2016) 1–9.
- [40] A.F. Bratton, S. Kim, C.E. Ellison, K.M. Miller, Thermomechanical and conductive properties of thiol-Ene poly(ionic liquid) networks containing backbone and pendant imidazolium groups, Ind. Eng. Chem. Res. 57 (2018) 16526–16536.
- [41] J.E. Bara, Versatile and scalable method for producing N-functionalized imidazoles, Ind. Eng. Chem. Res. 50 (2011) 13614–13619.
- [42] H. Helmboldt, M. Hierseman, Synthetic studies toward Jatrophane diterpenes from Euphorbia characias. Enantioselective synthesis of (-)-15-O-acetyl-3-O-propionyl-17-norcharaciol, J. Org. Chem. 74 (2009) 1698–1708.
- [43] L. Cammarata, S.G. Kazarian, P.A. Salter, T. Welton, Molecular states of water in room temperature ionic liquids, Phys. Chem. Chem. Phys. 3 (2001) 5192–5200.
- [44] K. Shanmuganathan, S.M. Elliot, A. Lane, C.J. Ellison, Highly stretchable thermoset fibers and nonwovens using thiol-ene photopolymerization, ACS Appl. Mater. Interfaces 6 (2014) 14259–14265.
- [45] B.D. Mather, K.M. Miller, T.E. Long, Novel Michael addition networks containing poly(propylene glycol) telechelic oligomers, Macromol. Chem. Phys. 207 (2006) 1324–1333.
- [46] H.K. Roobottom, H.D.B. Jenkins, Thermochemical radii of complex ions, J. Chem. 76 (1999) 1570–1572.
- [47] M.C. Simoes, K.J. Hughes, D.B. Ingham, L. Ma, M. Pourkashanian, Estimation of the thermochemical radii and ionic volumes of complex ions, Inorg. Chem. 56 (2017) 7566–7573.
- [48] J.G. Huddleston, A.E. Visser, W.M. Reichert, H.D. Willauer, R.D. Rogers, Characterization and comparison of hydrophilic and hydrophobic room temperature ionic liquids incorporating the imidazolium cation, Green Chem. 3 (2001) 156–164.
- [49] C. Maton, N. De Vos, C.V. Stevens, Ionic liquid thermal stabilities: decomposition mechanisms and analysis tools, Chem. Soc. Rev. 42 (2013) 5963–5977.
- [50] R. Lungwitz, S. Spange, Hydrogen bond accepting (HBA) scale for anions, including room temperature ionic liquids, New J. Chem. 32 (2008) 392–394.
- [51] U.G. Brauer, A.T. De La Hoz, K.M. Miller, The effect of counteranion on the physicochemical and thermal properties of 4.methyl-1-propyl-1,2,4-triazolium ionic liquids, J. Mol. Liq. 210 (2015) 286–292.
- [52] C. Jangu, J.H. Wang, D. Wang, S. Sharick, J.R. Heflin, K.I. Winey, R.H. Colby, T. E. Long, Well-defined imidazolium ABA triblock copolymers as ionic-liquid-containing electroactive membranes, Macromol. Chem. Phys. 215 (2014) 1319–1331.
- [53] R.J. Klein, S. Zhang, S. Dou, B.H. Jones, R.H. Colby, J. Runt, Modeling electrode polarization in dielectric spectroscopy: ion mobility and mobile ion concentration of single-ion polymer electrolytes, J. Chem. Phys. 124 (2006) 144903–144908.

- [54] E.W. Stacey, C.P. Gainaru, M. Gobet, Z. Wojnarowska, V. Bocharova, S. G. Greenbaum, A.P. Sokolov, Fundamental limitations of ionic conductivity in polymerized ionic liquids, Macromolecules 51 (2018) 8637–8645.
- [55] N.S. Schauser, D.J. Grzetic, T. Tabassum, G.A. Kliege, M.L. Le, E.M. Susca, S. Antoine, T.J. Keller, K.T. Delaney, S. Han, R. Seshardi, G.H. Fredrickson, R. A. Segalman, The role of backbone polarity on aggregation and conduction of ions in polymer electrolytes, J. Am. Chem. Soc. 142 (2020) 7055–7065.
- [56] Y. Ye, J. Elabd, Anion exchanged polymerized ionic liquids: high free volume single ion conductors, Polymer 52 (2011) 1309–1317.
- [57] C.M. Evans, G.E. Sanoja, B.C. Popere, R.A. Segalman, Anhydrous proton transport in polymerized ionic liquid block copolymers: roles of block length, ionic content, and confinement, Macromolecules 49 (2016) 395–404.
- [58] U.H. Choi, L.R. Middelton, M. Soccio, C.F. Buitrago, H. Aitken, H. Masser, K. B. Wagener, K.I. Winey, J. Runt, Dynamics of precise ethylene ionomers containing ionic liquid functionality, Macromolecules 48 (2015) 410–420.
- [59] J.R. Macdonald, Theory of ac space-charge polarization effects in photoconductors, semiconductors, and electrolytes, Phys. Rev. 92 (1953) 4–17.
- [60] R. Coelho, On the static permittivity of dipolar and conductive media an educational approach, J. Non-Cryst. Solids 131 (1991) 1136–1139.
- [61] D. Fragiadakis, S. Dou, R.H. Colby, J. Runt, Molecular mobility, ion mobility, and mobile ion concentration in poly(ethylene oxide)-based polyurethane ionomers, Macromolecules 41 (2008) 5723–5728.
- [62] T. Kakiuchi, Electrochemical aspects of ionic-liquid/water two-phase systems, Anal. Chem. 79 (2007) 6442–6449.
- [63] Y.A. Elabd, Ion transport in hydroxide conducting block copolymers, Mol. Syst. Des. Eng. 4 (2019) 519–530.